Biochemical and Genetic Analysis of *ANK* in Arthritis and Bone Disease

Kyle A. Gurley, Richard J. Reimer, and David M. Kingsley

Mutations in the progressive ankylosis gene (*Ank/ANKH*) cause surprisingly different skeletal phenotypes in mice and humans. In mice, recessive loss-of-function mutations cause arthritis, ectopic crystal formation, and joint fusion throughout the body. In humans, some dominant mutations cause chondrocalcinosis, an adult-onset disease characterized by the deposition of ectopic joint crystals. Other dominant mutations cause craniometaphyseal dysplasia, a childhood disease characterized by sclerosis of the skull and abnormal modeling of the long bones, with little or no joint pathology. *Ank* encodes a multiple-pass transmembrane protein that regulates pyrophosphate levels inside and outside tissue culture cells in vitro, but its mechanism of action is not yet clear, and conflicting models have been proposed to explain the effects of the human mutations. Here, we test wild-type and mutant forms of ANK for radiolabeled pyrophosphate-transport activity in frog oocytes. We also reconstruct two human mutations in a bacterial artificial chromosome and test them in transgenic mice for rescue of the *Ank* null phenotype and for induction of new skeletal phenotypes. Wild-type ANK stimulates saturable transport of pyrophosphate ions across the plasma membrane, with half maximal rates attained at physiological levels of pyrophosphate. Chondrocalcinosis mutations retain apparently wild-type transport activity and can rescue the joint-fusion phenotype of *Ank* null mice. Craniometaphyseal dysplasia mutations do not transport pyrophosphate and cannot rescue the defects of *Ank* null mice. Furthermore, microcomputed tomography revealed previously unappreciated phenotypes in *Ank* null mice that are reminiscent of craniometaphyseal dysplasia. The combination of biochemical and genetic analyses presented here provides insight into how mutations in *ANKH* cause human skeletal disease.

Mineral deposition is a highly regulated process in vertebrates and is normally confined to the bony skeleton. Excess or ectopic mineral deposition occurs in a large fraction of the elderly population and is a phenotype of many specific diseases. Recent progress in both mouse and human genetics has identified a number of genes that play key roles in controlling mineral deposition in body tissues.[1–17] Mutations in several of these genes affect the generation or degradation of pyrophosphate (PPi) and lead to defects in crystal formation throughout the skeleton. At low levels, PPi is a potent inhibitor of calcium phosphate crystal formation.[18,19] It is even used commercially to inhibit mineralization, including its use as an ingredient in most forms of tartar-control toothpaste. In contrast, when present at high levels, PPi itself can precipitate with calcium ions to form an alternative type of crystal called "calcium pyrophosphate dihydrate" (CPPD).[20–22]

ANKH (or the mouse ortholog *Ank*) encodes a novel 492-aa multipass transmembrane protein (ANKH/ANK) that is hypothesized to transport PPi ions across the plasma membrane to the extracellular environment.[3] The importance of *Ank* was first elucidated in mice when it was shown that a spontaneous mutation called "progressive ankylosis" (*ank*) causes hydroxyapatite—$Ca_5(PO_4)_3(OH)$—mineral deposition in the articular cartilage and synovial fluid.[3,15] Crystal deposition begins at age ~3–4 wk and ultimately leads to immobility due to the complete fusion of almost every joint in the body.[23,24] The nonsense *ank* mutation results in the C-terminal truncation of the ANK protein by 53 aa.[3] We recently reported that mice homozygous for the *Ank* null allele (Ank^{null}) exhibit the same phenotype as do *ank* mice.[25]

The discovery of ANK and its role in joint maintenance led to the discovery of mutations in *ANKH* that are associated with a variety of skeletal defects in humans.[8,10,11,17,26–31] Four dominant mutations in *ANKH* cause familial chondrocalcinosis (CCAL2 [MIM 118600]), an adult-onset mineral-deposition disease.[10,17,30] Like *ank* mice, patients with CCAL2 experience ectopic crystal deposition in the articular cartilage and synovial fluid. However, in contrast to the hydroxyapatite crystals deposited in the joints of young *ank* mice, the crystals found in the joints of patients with CCAL2 are composed of CPPD and do not appear until the 3rd or 4th decade of life. The familial CCAL2 mutations cluster at the N terminus of the ANKH protein, and each results in a change of only 1–4 aa.

Six additional dominant mutations in *ANKH* were discovered in studies of craniometaphyseal dysplasia (CMD [MIM 123000]) in humans.[8,11] CMD is a rare condition characterized by hyperostosis and sclerosis of the skull, together with flaring and abnormal modeling of the metaphyses of the long bones. In striking contrast to the joint

From the Department of Developmental Biology (K.A.G.; D.M.K.), Department of Neurology and Neurological Sciences (R.J.R.), and Howard Hughes Medical Institute (D.M.K.), Stanford University School of Medicine, Stanford

Received July 20, 2006; accepted for publication September 26, 2006; electronically published October 16, 2006.

Address for correspondence and reprints: Dr. David Kingsley, Department of Developmental Biology, Beckman Center B300, Stanford University School of Medicine, 279 Campus Drive, Stanford, CA 94305. E-mail: kingsley@cmgm.stanford.edu

Am. J. Hum. Genet. 2006;79:1017–1029. 0002-9297/2006/7906-0004$15.00

diseases caused by the recessive mouse *ank* mutation and the dominant human CCAL2 mutations, patients with CMD have normal joints. All of the CMD mutations affect single amino acids and cluster in a small region of the ANKH protein that is distinct from the region affected in patients with CCAL2.

In addition to the protein-coding mutations that cause CCAL2 and CMD, noncoding *ANKH* polymorphisms associate with ankylosing spondylitis, a devastating disease that results in fusions of the spine, and with hand bone size and geometry.[26–29] Despite the clear involvement of *ANKH* in numerous skeletal defects, very little is known about how mutations in the ANKH protein affect its function.

The ANK protein contains 8–12 predicted transmembrane helices and is present on the plasma membrane.[3] Overexpression of *Ank* in tissue culture cells leads to an increase in total levels of extracellular PPi.[3,31] Conversely, loss of ANK activity in mutant cells leads to a decrease in extracellular PPi levels,[3,32,33] which translates in vivo to increased mineral formation in articular cartilage and joints. The multiple-pass transmembrane sequence of the ANK protein suggests that it may act directly as a PPi transporter. However, all previous measurements of ANK function have relied on bulk PPi measurements from cells and media after several days in culture. No experiments have directly tested whether ANK stimulates the actual movement of PPi across the plasma membrane.

It is also not clear whether the different human mutations act by loss- or gain-of-function mechanisms. Human CCAL2 mutations may be weak hypermorphic mutations, because they cause elevated levels of PPi in synovial fluid and predispose to deposition of CPPD crystals.[10,34–36] However, two different groups tested the activity of these mutant alleles by overexpression in tissue culture cells and reported different results, which led to different conclusions about their function.[10,31] Importantly, this has led some investigators to question whether the effect of ANK on PPi levels is relevant to its role in human disease.[31]

Human CMD mutations are interesting because they cluster in a small region of the ANKH protein and cause thickening of bones without major effects on joints. Conflicting models have been proposed about the possible effects of these mutations on ANKH activity, with different groups suggesting that the CMD alleles act as hypermorphic, hypomorphic, or dominant negative mutations.[8,11] No biochemical measurements of the activity of CMD-mutant proteins have been described. Finally, no in vivo assays have been reported that examine the activity of the CCAL2 or CMD *ANKH* alleles in mice.

To better understand the normal function of the ANK protein and its role in human disease, we used a combination of radiotracer flux experiments and transgenic mice to characterize the activity of wild-type and mutant ANK proteins. The combined biochemical and genetic data confirm an important role for ANK in PPi transport and provide a model to explain how different types of mutations in *ANKH* lead to human disease.

Material and Methods

Molecular Biology

The human ANKH and mouse ANK proteins are both 492 aa in length and are 98% identical, differing at only 8 aa. All known human alleles affect conserved amino acids. Variant alleles were therefore introduced into the mouse *Ank* cDNA. The P5T base-pair change was 13C→A. The M48T base-pair change was 143T→C. The C331R base-pair change was 991T→C. The G389R base-pair change was 1165G→A. For expression in *Xenopus* oocytes, cDNA samples were subcloned from pCDNA3 into pOX, which contains 5′ and 3′ UTR sequences from frog beta-globulin. Mutations were introduced by PCR, and all constructs were confirmed by sequencing.

Expression of ANK in X. laevis *Ooctyes*

Capped mRNA (cRNA) was transcribed in vitro with T3 RNA polymerase (mMESSAGE mMACHINE kit [Ambion]) from *Not*I-linearized templates and was resuspended in nuclease-free water. Oocytes were surgically collected from animals anesthetized under 0.17% tricaine and were incubated for 1 h, with shaking, in ND96 (in mM: 96 NaCl, 2 KCl, 1.8 $CaCl_2$, 1 $MgCl_2$, and 5 HEPES [pH 7.6]) and 2 mg/ml of collagenase. Healthy stage V and VI oocytes were injected with 80 nl of RNase-free water or 8–16 ng of cRNA. Healthy injected oocytes were given fresh ND96 daily and were maintained at 18°C before uptake studies were performed.

Membrane-Enriched Protein Lysates and Cell-Surface Biotinylation

Proteins were isolated from healthy oocytes 2–9 d after injection. Groups of 10–30 oocytes were homogenized in 500 μl ice-cold hypotonic lysis buffer (15 mM tris [pH 6.8]) plus Complete Mini protease inhibitors (Roche Applied Science). To remove yolk proteins, the homogenate was mixed 1:1 with 1,1,2-trichlorofloroethane (Sigma), was vortexed, and was centrifuged at 3,600 *g* for 10 min at 4°C. Membranes were pelleted by centrifugation and were resuspended in 10–15 μl of lysis buffer with protease inhibitors. Protein concentration was determined by the method of Lowry.

Cell-surface biotinylation experiments were performed 2 d after injection. Pools of 15–20 healthy oocytes were labeled with 2 mM EZ-Link-Sulfo-NHS-LC-Biotin (Pierce Biotechnology), as per the manufacturer's instructions. After removal of yolk proteins from the lysates, a 20-μl aliquot was collected for total protein. The remaining lysates were incubated with streptavidin beads (Pierce) for 1–8 h at 4°C. Precipitated proteins were eluted in SDS loading buffer at 55°C–65°C for 20 min.

Western Blots

Proteins were separated by 10% SDS-PAGE. The primary antibodies were rabbit-αANK ($Ab3^3$) and mouse-αPDI (protein disulphide isomerase) (Stressgen Bioreagents). Immunoblotting and detection of horseradish peroxidase–conjugated secondary antibodies (Santa Cruz Biotechnology) by enhanced chemiluminescence (Amersham) were done according to manufacturers' instructions. For surface-labeling experiments, the blots were probed

with αANK, were stripped as recommended, and were reprobed with αPDI.

PPi Uptake Assays

Uptake experiments were conducted at room temperature 2 d after cRNA injection. Groups of 7–9 oocytes were washed in fresh ND96 and were incubated in 120 μl of transport buffer (ND96 containing ^{33}PPi [Perkin Elmer Custom Synthesis] to a final specific activity of 50 Ci/mmol) at room temperature for 20 min, unless otherwise indicated. Uptake was stopped by washing three times in 2 ml of ice-cold ND96. Oocytes were lysed individually in 150 μl of 10% SDS, and radioactive counts were determined after adding 4 ml of liquid scintillation fluid. Each final data point was determined by removing the highest oocyte count and the lowest oocyte count from each pool (7–9 oocytes) and averaging the results from at least three independent experiments, each from a separate batch of oocytes. Thin-layer chromatography showed that no detectable hydrolysis of PPi to Pi occurred in transport buffer incubated with oocytes during the time periods used for PPi uptake assays (data not shown).

Generation of BAC Transgenic Mice

Using homologous recombination in *Escherichia coli*,[37] we modified a BAC that contains the *Ank* locus and was used elsewhere as a transgene to rescue mutant *ank* animals.[3] For both of the *Ank*^{M48T} and *Ank*^{G389R} alleles, a tetracycline cassette was inserted into the appropriate site and then was replaced with the intended base-pair mutation.

The primers used to amplify the tetracycline cassette and introduce homology arms were: for *Ank*^{M48T}-tet, 5′-GGCCTTGAACCGGGGCATCGCTGCAGTCAAGGAGGATGCAGTAGAAGATCTATGATTCCCTTTGTCAACAG-3′ (forward) and 5′-TCAGGGTGTGGAAGACGGCAGCGATGGCACCGGCCACCACCATGCAAGCTTATGATGATGATGTGCTTAAAAAC-3′ (reverse); for *Ank*^{G389R}-tet, 5′-CACACCCTTCTCTCCTCAGTGACTGTGAGAGCTCATCTCACTAGATCTATGATTCCCTTTGTCAACAG-3′ (forward) and 5′-CAGGTACGGCAGGACCACAAGGCTGGTGATGAGGACGATGATAAGCTTATGATGATGATGTGCTTAAAAAC-3′ (reverse). The template used for the replacement amplicon was an *Ank* cDNA vector containing the desired point mutation (see the "Molecular Biology" section). The primers were: for *Ank*^{M48T}, 5′-GCGGATCCGGCCTTGAACCGGGGCAT-3′ (forward) and 5′-GCGGATCCCAGGGTGTGGAAGACGGCA-3′ (reverse); for *Ank*^{G389R}, 5′-GCGGATCCCACACCCTTCTCTCCTCAGTGACTGTGAGAGCTCATCTCACT-3′ (forward) and 5′-CGCGGATCCCAGGTACGGCAGGACCACA-3′ (reverse).

Pulse-field gel electrophoresis, DNA fingerprinting, and PCR/DNA sequencing were used to verify BAC integrity and to confirm that the appropriate changes were made. The modified BACs are referred to in the text as "BAC-*Ank*^{M48T}" and "BAC-*Ank*^{G389R}."

Circular BAC DNAs were dialyzed in microinjection buffer (10 mM Tris [pH 7.4] with 0.15 mM EDTA [pH 8.0]), were adjusted to 1 ng/μl, and were injected into the pronuclei of fertilized eggs from FVB/N or B6CBAF1/J mice by the Stanford Transgenic Facility. Transgenic founder mice were identified by PCR, with use of BAC-specific primers 5′-CTATAGTGTCACCTAAATAGC-3′ (forward) and 5′-GGTTCGCGTTGGCCGATT-3′ (reverse). Founder mice generated on the hybrid background were first bred to FVB/N mice to introduce a polymorphic D15Mit180 allele near the *Ank* locus that was used for genotyping in the rescue studies.

BAC-positive mice were crossed with +/*Ank*^{null} mice for 2 generations to produce F2 animals that were assessed for rescue and were phenotyped. Genotyping primers for the *Ank*^{null} allele at the endogenous *Ank* locus were described elsewhere.[25] The marker D15Mit180 was used to genotype for rescue (5′-TTGCCATTGCAATGCATG-3′ [forward] and 5′-GGTCAGCCATGAAAGCATAA-3′ [reverse]). All mice were on mixed backgrounds, including FVB/N, CBA/J, C57BL/6, C3H/HeJ, and 129S1/SvImJ. All analyzed mice were littermates and/or siblings from the same mating.

Verification of Transgene Expression

To screen transgenic lines for expression of the introduced alleles, RNA was collected from spleen, liver, and kidney, with use of the RNAqueous-4-PCR kit (Ambion), and reverse transcription was performed using random decamers. PCR primers for BAC-*Ank*^{M48T} were 5′-GGCCTTGAACCGGGGCAT-3′ (forward) and 5′-CAGCTCTGGGCCGCTCCTGT-3′ (reverse) and generated a 589-bp product. RT-PCR products from +/*Ank*^{null};BAC-*Ank*^{M48T} animals were directly sequenced, to detect transgene expression. The sequencing primer (5′-ACAGACTCATCCACATGATGC-3′) recognizes *Ank* exon 3 and does not hybridize with the *Ank*^{null} allele from the endogenous locus. Therefore, the apparent ratio of endogenous *Ank* transcripts to transgenic *Ank* transcripts was 1:1, which enabled the detection of transgene transcripts from the sequencing chromatograms.

Primers for BAC-*Ank*^{G389R} were 5′-TGGCTCTGATCCTGGCCACG-3′ (forward) and 5′-CTTCTCTCATCTCTACGATGT-3′ (reverse) and generated a 738-bp product. The wild-type product can be digested with *Fok*I into two bands, 435 bp and 303 bp. The G389R allele eliminates this restriction site, and PCR products from this allele are not digested with *Fok*I.

Mouse Phenotyping

Mice were euthanized at age 6 wk, 6 mo, or 1.5 years. Knee analysis was performed using both *Ank*^{M48T} lines that rescued the *Ank* null phenotype. Skull and femur analysis was performed on two of the four *Ank*^{G389R} lines that expressed the transgene as assayed by RT-PCR. Skulls, right forepaws, right hindpaws, and right legs were fixed in 10% buffered formalin, were rinsed in PBS, and then were transferred to 70% ethanol for long-term storage at 4°C. Forepaws, legs, and skulls were scanned and evaluated by microCT (μCT) in 70% ethanol. μCT analysis was performed using a μCT-40 (ScanCo Medical) operated at a tube potential of 45 kV and a tube current of 177μA, with use of a 0.30-s integration with 2× averaging. A threshold to distinguish bone from soft tissue was empirically determined using wild-type specimens. Voxel sizes were 8 μm^3 for mouse forepaws, 16 μm^3 for femurs, and 16 μm^3 for skulls from mice sacrificed at age 6 wk and were 20 μm^3 for skulls from mice sacrificed at age 6 mo. All six F2 genotypes from the cross shown in figure 3 were analyzed.

To assign thickness values for each point in the skull, files containing the coordinates for all pixels of the skull were processed as described elsewhere.[38–40] In brief, for each pixel, the diameter of the largest possible bone-containing sphere was calculated, and each pixel was assigned a thickness value. This process generated (1) a histogram of the number of pixels that were assigned to each bin of thickness values and (2) a skull-thickness map that shows the assigned thickness values in three-dimensional space.

For distal femurs, evaluation of cancellous bone in the metaphyseal region was performed on 50 two-dimensional slices (800 μm), starting at the base of the growth plate and moving prox-

imally toward the diaphysis. The cortex of the metaphysis was evaluated for the 20 most-proximal slices that were used for the cancellous evaluation.

Statistics

Significance was evaluated by *t* test versus control values or analysis of variance (ANOVA) with Bonferroni's multiple-comparison test. All statistics, including nonlinear and linear regression, were performed using the Prism software package (Graphpad Software). Data are presented as mean ± SE.

Results

ANK-Stimulated PPi Flux across the Plasma Membrane

An *X. laevis* heterologous expression system was used to test whether the ANK protein stimulates movement of PPi across the plasma membrane. It is hypothesized that ANK mediates transport of PPi out of cells, but we were unable to directly measure PPi efflux from oocytes because of technical limitations. However, we were able to take advantage of the bidirectionality of transport and instead measured uptake, an approach that has proven successful in the characterization of other transporters.[41–48]

Ank in vitro–transcribed cRNA was injected into *Xenopus* oocytes, which expressed the ANK protein within 2 d (fig. 1*A* and data not shown). ANK-expressing oocytes were incubated in 1 μM radiolabeled PPi for various amounts of time and showed linear uptake over the course of 1 h (fig. 1*B*). After 10 min, uptake by ANK-expressing oocytes was already 16.3-fold greater than uptake by water-injected controls. Linear regression revealed an uptake rate of 1.54 ± 0.04 fmol PPi per oocyte per min. This is equivalent to a turnover rate of 2.57 ± 0.067 × 10^6 PPi ions per s per oocyte. Uptake was then measured at the 20-min time point for a variety of PPi concentrations. Plotting the rate of transport versus substrate concentration revealed that the rate of ANK-dependent PPi uptake was saturable with an apparent Michaelis-Menten constant (Km) of 1.33 ± 0.59 μM (fig. 1*C*).

To assess whether the disease-causing *Ank* mutations affect ANK-stimulated PPi-transport activity, oocytes were injected with the appropriate cRNAs, and PPi flux was measured at near-saturating (7 μM) conditions. The tested CCAL2 mutant proteins (P5T and M48T) displayed wild-type levels of transport activity, and saturation curves revealed that neither apparent Km was significantly different from that measured in parallel for wild-type ANK (fig. 2*A* and 2*B*). In contrast, the *ank* truncation protein (E440X) and both of the tested CMD mutant proteins (C331R and G389R) showed little to no PPi-transport activity (fig. 2*A*). This was not due to mislocalization, since surface biotinylation experiments confirmed that, with the exception of the truncated *ank* protein—which is missing the epitope recognized by the anti-ANK antibody and served as a control for antibody specificity—the wild-type and mutant ANK proteins were present on the oocyte plasma membrane (fig. 2*D*).

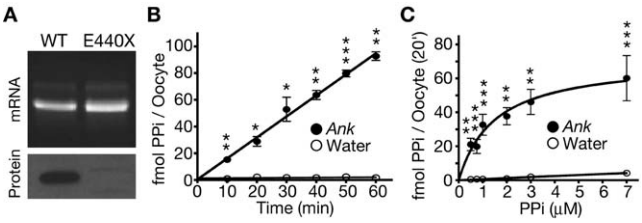

Figure 1. ANK stimulation of PPi translocation across the plasma membrane. *A,* Agarose gel of wild-type (WT) *Ank* and mutant *ank* cRNAs, with western blot of membrane-enriched protein lysates from *Xenopus* oocytes 3 d after cRNA injection. The cRNA appears intact, and the ANK protein was detected. The mutant *ank* cRNA encodes a truncated protein (E440X) that does not contain the C-terminal epitope recognized by the ANK antibody and therefore served as a control for antibody specificity. *B,* Time course of PPi uptake by oocytes in transport buffer with 1 μM ^{33}PPi. After subtracting uptake by water-injected controls, the calculated rate of ANK-dependent transport is 1.54 ± 0.04 fmol per oocyte per min ($n = 3$). *C,* Rate of ANK-stimulated PPi transport as a function of substrate concentration. The transport rate was saturable, and the apparent Km was 1.33 ± 0.59 μM after subtracting uptake by water-injected controls ($n = 8$). A single asterisk (*) indicates $P < .05$; a double asterisk (**) indicates $P < .01$; a triple asterisk (***) indicates $P < .001$.

The inability of the C331R and G389R mutant proteins to transport PPi, coupled with the dominant inheritance of CMD, suggested that these two alleles might act as dominant negatives. Oocytes co-injected with wild-type and mutant (C331R or G389R) cRNA exhibited significantly less uptake than did those injected with wild-type cRNA alone (fig. 2*C*). When coexpressed with the wild-type ANK protein, the CMD-mutant proteins (C331R and G389R) did not grossly affect ANK surface expression (fig. 2*D*).

In Vivo Test of Human Disease Alleles

Transgenic mice were generated to test the effect of the human mutations on ANK activity in vivo and to attempt to recapitulate CCAL2 and CMD in mice. A mouse BAC that was shown elsewhere to rescue the *ank* phenotype[3] was modified by homologous recombination in bacteria[37] to incorporate the appropriate base-pair mutations in the *Ank* ORF. One CCAL2 BAC (BAC-Ank^{M48T}), one CMD BAC (BAC-Ank^{G389R}), and one unmodified BAC were used to establish multiple transgenic founders from independent integrations. Founders were bred to +/Ank^{null} mice for 2 generations (fig. 3*A*), and transgenic lines were screened by RT-PCR performed on multiple organs to identify those that expressed the transgene (fig. 3*B* and 3*C* and data not shown).

To test the function of the M48T (CCAL2) and G389R (CMD) ANK-mutant proteins in vivo, we used rescue of the *Ank* null phenotype as an assay. When wild-type ANK is provided by a transgenic BAC in *ank*-mutant mice, the severe joint-fusion phenotype is greatly reduced or elim-

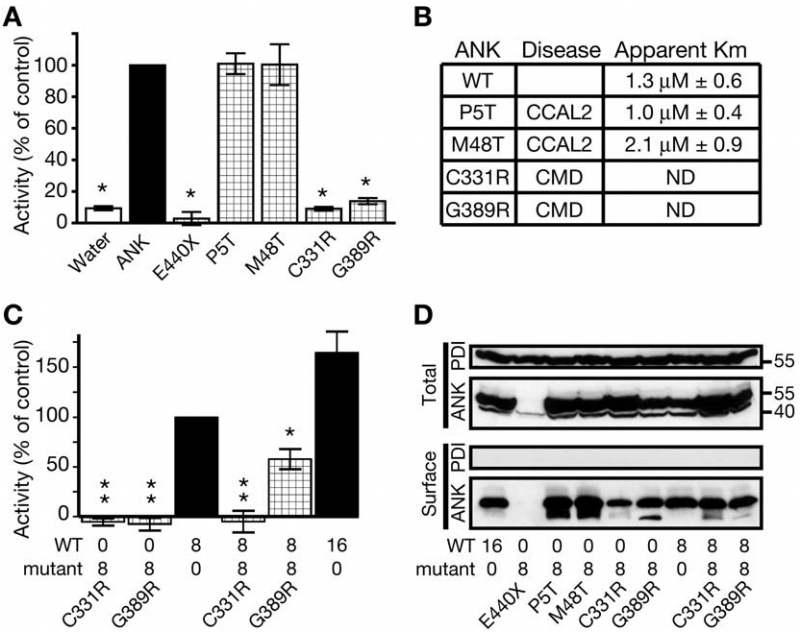

Figure 2. PPi-transport assay with disease-causing *Ank* alleles. *A,* Oocytes expressing mutant *Ank* alleles were assayed for PPi uptake over a 20-min period at near-saturating conditions (7 μM). Note that oocytes expressing either of the CCAL2 proteins (P5T or M48T) exhibited wild-type uptake, whereas oocytes expressing the truncated ank protein (E440X) or either of the CMD proteins (C331R or G389R) exhibited little to no uptake. An asterisk (*) indicates $P \leq .0005$ versus wild-type control; $n \geq 3$). *B,* Apparent Km measurements for wild-type (WT) and CCAL2 proteins. Neither mutant was significantly different from wild-type controls tested in parallel ($n = 4$ for each mutant allele; $n = 8$ for wild type). ND = not determined. *C,* Oocytes were co-injected with a 1:1 ratio of wild-type and mutant *Ank* cRNA. Both CMD proteins (C331R and G389R) had a statistically significant dominant negative effect, although the effect from C331R was stronger. Numbers on the *X*-axis are ng of cRNA injected. Values from water-injected oocytes were subtracted from experimental values. A single asterisk (*) indicates $P < .05$; a double asterisk (**) indicates $P < .003$ versus wild-type control; $n = 4$). *D,* Surface biotinylation assays for plasma membrane localization of wild-type and mutant ANK proteins when expressed in *Xenopus* oocytes. All of the tested variants were detected at the surface, with the exception of the truncated ank protein, which served as a control for antibody specificity. The C331R mutant protein showed decreased surface expression compared with wild type. When the dominant negative CMD mutant proteins (C331R and G389R) were coexpressed with wild-type ANK, they did not grossly affect its surface expression. A smaller band is seen in some lanes, but its presence was inconsistent in multiple trials, and we were unable to determine its nature. PDI localizes to the endoplasmic reticulum and served as a negative control for surface expression.

inated.[3] We recently showed that *Ank* null mice exhibit the same phenotype as do *ank* mice.[25] Therefore, if a mutant ANK protein provided by a modified BAC transgene is active (transports PPi), no joint-fusion phenotype should be observed in transgenic *Ank* null mice. If the introduced mutant ANK protein is inactive, these mice should instead exhibit joint fusion.

For all tested BAC clones (wild type, M48T, and G389R), those lines that did not express the transgene, as assessed by RT-PCR, also did not rescue the joint phenotypes (zero of five lines tested). For the wild-type and M48T BAC clones, most lines that expressed the transgene showed significant rescue of joint phenotypes (three of four lines tested).

Control experiments showed that expression of the wild-type mouse BAC significantly reduced the severity of joint defects in *Ank*-knockout mice, as reported elsewhere for animals homozygous for the classical Ank^{ank} allele.[3] Partial rescue included delayed onset (by at least 2 wk in two mice and at least 2 mo in five mice) and full rescue of some joints accompanied by complete fusion of other joints. Despite both individual and regional variation, the phenotypes of all eight transgenic *Ank* null mice were much less severe than were those of nontransgenic null littermates.

Two of three transgenic lines that expressed the M48T CCAL2 allele, as assessed by RT-PCR, also showed significant rescue of *Ank* null phenotypes. For BAC-Ank^{M48T} line 1, expression of the M48T transgene did not rescue the *Ank* null phenotype (zero of six mice). However, expression of this CCAL2-mutant protein in line 2 conferred a partial rescue reminiscent of the rescue observed using wild-type ANK. This included a delay of disease onset that eventually led to the fusion of some joints but left other joints unaffected (9 of 12 mice). In all nine cases of partial rescue for line 2, the phenotype of transgenic *Ank* null mice was much less severe than was the phenotype of nontransgenic null littermates. Finally, BAC-Ank^{M48T} line

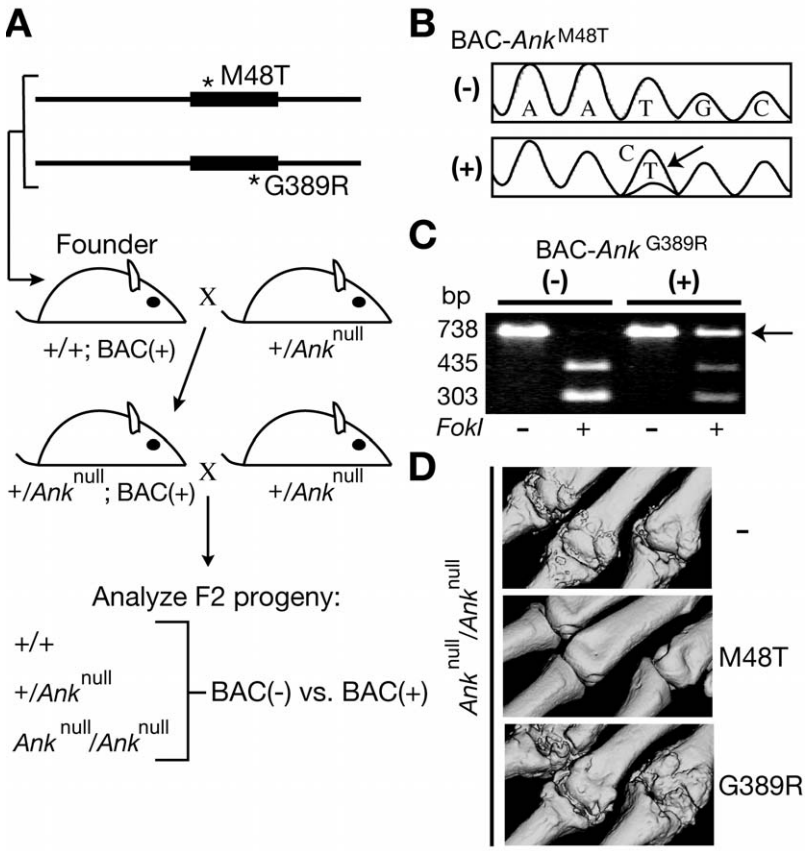

Figure 3. Transgenic expression of *Ank* disease alleles in mice. *A,* Breeding strategy. BACs were modified by homologous recombination in bacteria and were used to generate transgenic founders. Founders were crossed for 2 generations with $+/Ank^{null}$ mice. *B–C,* Analysis of RT-PCR products from $+/Ank^{null}$;BAC+ and control $+/Ank^{null}$;BAC− mice. In panel B, direct sequencing confirmed the expression of the Ank^{M48T} allele, which is derived from a T→C bp change (*arrow*). In panel C, restriction digests confirmed the expression of the Ank^{G389R} allele (*arrow*), which does not contain an *Fok*I site. The wild-type allele was detected in all cases. *D,* μCT-derived volumetric reconstructions of digits 2–4 of the right forepaw at age 6 wk. Whereas the Ank^{M48T} allele rescued the *Ank* null phenotype in two of three transgenic lines, the Ank^{G389R} allele did not rescue in any of the four lines. As a control, the wild-type ANK protein expressed from an unmodified BAC rescued the *Ank* mutant phenotypes in four of four transgenic lines[3] (and data not shown).

3 exhibited full rescue, since *Ank* null mice expressing the M48T protein still showed no signs of crystal formation, joint fusion, or immobility by age 6 mo (16 of 16 mice), a time when their nontransgenic *Ank* null littermates were completely immobile (fig. 3*D*).

In contrast to results with both wild-type ANK and M48T (CCAL2) BACs, introduction of a BAC carrying the G389R (CMD) mutation failed to rescue the joint-fusion phenotype of *Ank* null mutants. A total of 52 *Ank* null animals carrying the G389R BAC were tested, including 6, 9, 15, and 22 from four independent transgenic lines. Lack of rescue was not due to failure to express the G389R allele, since RT-PCR analysis confirmed expression of the altered allele (fig. 3*C*). Interestingly, these in vivo rescue data parallel the in vitro oocyte experiments in which CCAL2-mutant proteins stimulated wild-type levels of PPi transport and the CMD mutant proteins were unable to stimulate PPi transport.

*Knee Analysis of BAC-*Ank^{M48T} *Transgenic Mice*

To test for late-onset phenotypes in animals with the CCAL2 mutation, mice aged 6 mo or 1.5 years with the genotypes (1) +/+, (2) +/+;BAC-Ank^{M48T}, (3) $+/Ank^{null}$, and (4) $+/Ank^{null}$;BAC-Ank^{M48T} were analyzed by μCT for the presence of abnormal crystal content in the knee, a major load-bearing joint of the animal and a common site of CPPD crystal deposition in humans. There were no signs of ectopic crystals or osteoarthritis in any of the mice scanned at age 6 mo. By age 1.5 years, some mice exhibited signs of osteoarthritis in the knee, including ectopic crystal formation, osteophyte formation, and enlarged/expanded menisci. However, each of these features also occurred spontaneously in control animals, and we could detect no significant increase in incidence that was attributable to the presence of the BAC-Ank^{M48T} transgene.

This analysis was performed using both Ank^{M48T} lines that rescued the *Ank* null phenotype.

*Skull and Femur Analysis of BAC-*Ank^{G389R} *Transgenic and* Ank *Null Mice*

Because CMD affects skull and femur morphology in humans, we used μCT to evaluate the skulls and femurs of mice with the genotypes (1) +/+, (2) +/+;BAC-Ank^{G389R}, (3) +/Ank^{null}, (4) +/Ank^{null};BAC-Ank^{G389R}, (5) Ank^{null}/Ank^{null}, and (6) Ank^{null}/Ank^{null};BAC-Ank^{G389R} (fig. 4*A*). For most measurements, no significant differences were seen between groups that differed only in the presence or absence of the BAC transgene. However, numerous important differences were observed between wild-type and *Ank* null animals, and many of these differences suggest that reduced function of ANK in mice can recapitulate some of the phenotypic defects in CMD. Skulls of *Ank* null mice, aged 6 mo, were 0.71 mm narrower (7.1% difference; $P = .013$; $n = 6$ per genotype) and 1.22 mm shorter (4.7% difference; $P = .001$; $n = 6$ per genotype) than were skulls of wild-type mice. None of the scanned skulls exhibited ocular hypertelorism, paranasal bossing, obliteration of the nasal sinuses, or mandibular prognathism, all of which are characteristic features of CMD in humans. However, the foramen magnum of *Ank* null mice was significantly reduced in size compared with that of wild-type mice at age 6 mo (fig. 4*A*). A narrow foramen magnum is a documented feature of CMD in human patients.[49,50]

Like the skulls of patients with CMD, skulls of *Ank* null mice also contained thicker and denser bones than those of +/Ank^{null} or wild-type mice. A thickness value was calculated for each pixel from μCT skull scans (see the "Material and Methods" section). These data were used to generate (1) a spatially resolved and color-coded thickness map for each skull and (2) a histogram depicting the number of pixels with each thickness value (fig. 4*B*). Although marked sclerosis throughout the skull was not observed, this analysis revealed discrete anatomical regions that were thicker in the skulls of *Ank* null mice than in heterozygous or wild-type mice. The differences were also present in skulls from 6-wk-old mice (e.g., 0.3 mm^3 thickness counts of 76, 84, and 139 thousand pixels in +/+, +/Ank^{null}, and Ank^{null}/Ank^{null} mice, respectively).

Skulls from *Ank* null mice showed increased thickness in the basio-occipital bone, the tympanic bulla, and the petrous portion of the temporal bone, which houses the middle-ear bones and cochlea of the animal's hearing apparatus (fig. 4*B* and data not shown). Two-dimensional "slice" images revealed fusions between the middle-ear bones (fig. 4*C* and 4*D*). These fusions were already present in *Ank* null mice at age 6 wk, before the metacarpal-phalange joints of the hindpaw had ankylosed. Hearing loss due to hyperostosis, fixation, and fusion of the middle-ear bones is a well-documented feature of CMD, as are increased bone in the petrous portion of the temporal bone and increased bone in the cranial base.[49–53]

One of the most recognizable features of CMD in humans is a flaring or "clubbing" of the distal metaphysis of the femur, accompanied by a thin overlying cortex. A morphometric analysis revealed that the femurs of *Ank* null mice were slightly shorter and thinner than those of wild-type mice, but no significant flaring at the distal end of the femur was associated with any of the analyzed genotypes. Femurs were then evaluated for other features associated with bone remodeling. At the ages of 6 wk and 6 mo, Ank^{null}/Ank^{null} mice exhibited a reduced ratio of bone volume to tissue volume (BV:TV) in the metaphysis (fig. 5*B*). This was accompanied by a thin overlying cortex at age 6 wk (fig. 5*A*). Intriguingly, +/Ank^{null};BAC-Ank^{G389R} mice also displayed a significant decrease in BV:TV that was reminiscent of the decrease noted in *Ank* null animals (fig. 5*B*). Similar defects were not seen in +/Ank^{null} animals without the BAC transgene. Thus, in this sensitized genetic background, the presence of the G389R allele has a significant phenotypic effect on the femur. The Ank^{G389R} transgenic allele makes +/Ank^{null} mice more closely resemble Ank^{null}/Ank^{null} mice, consistent with a dominant negative effect on the development of phenotypes at this location.

Discussion

Although ANK activity is known to increase extracellular levels of PPi, it has remained unclear whether this is achieved by the translocation of PPi across the plasma membrane or by indirect effects on intracellular and extracellular PPi metabolism. We demonstrate here, to our knowledge for the first time, that ANK stimulates the actual transport of radioactive PPi across the plasma membrane. Our time-course and saturation studies reveal the basic kinetic parameters, rate, and Km of ANK-stimulated PPi transport. Both the saturation of transport rate near 10 μM PPi and the measured Km of 1.33 ± 0.59 μM support the physiological relevance of ANK activity in the *Xenopus* oocyte expression system. The affinity of the transporter is consistent with a mechanism for maintaining levels of PPi in human synovial fluid at ~1–10 μM[36,54–57] and with in vitro data that suggest that reduced or increased PPi levels lead to formation of calcium phosphate or calcium PPi dihydrate, respectively.[18,20,21,58–61]

Because ANK contains multiple transmembrane helices, is located on the plasma membrane, alters bulk levels of intracellular and extracellular PPi, and stimulates flux of radioactive PPi across oocyte membranes, it is likely to function directly as a PPi transporter[3,10,31–33] (and data presented here). However, it is formally possible that ANK functions indirectly to regulate the activity of a separate PPi transporter. Final proof that *Ank* encodes a transporter requires purification of the ANK protein and reconstitution in lipid membranes free of other cellular components. Nonetheless, the radioactive flux experiments presented here provide the most direct and sensitive assay yet de-

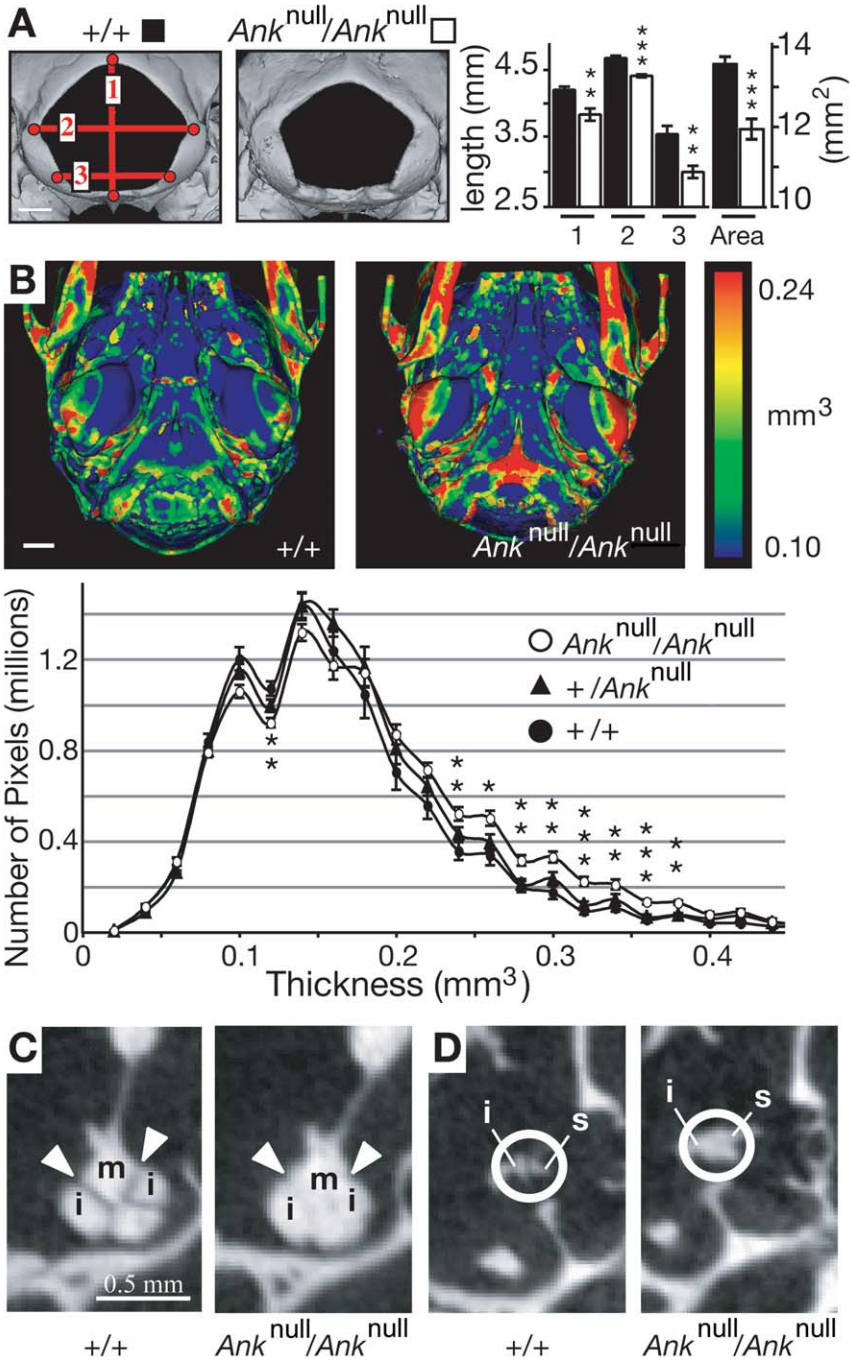

Figure 4. Skulls from *Ank*^{null}/*Ank*^{null} mice, which exhibit CMD-like features. *A,* Volumetric reconstructions of the foramen magnum from skulls of wild-type and *Ank* null mice aged 23 wk. The entryway for the spinal chord was significantly smaller in mutant mice ($n = 6$ mice for each genotype). Blackened bars indicate wild type; unblackened bars indicate *Ank* null; 1, 2, and 3 are the distances represented by red lines in the wild-type image. *B,* Ventral view of posterior region of skulls scanned by μCT. The skull images are color-coded for thickness, and the histogram plots the average number of pixels per thickness value for +/+, +/*Ank*^{null}, and *Ank*^{null}/*Ank*^{null} mice. The skulls of mice homozygous for the null allele are significantly thicker than those of controls. Note that the increase in thickness is not global but is instead restricted to discrete regions of the skull ($n = 6$ mice for each genotype). *C* and *D,* Two dimensional μCT "slice" images depicting the fusion of middle-ear bones in *Ank* null mice (m = malleus, i = incus, and s = stapes). A single asterisk (*) indicates $P < .05$; a double asterisk (**) indicates $P < .01$; a triple asterisk (***) indicates $P < .001$ versus wild type.

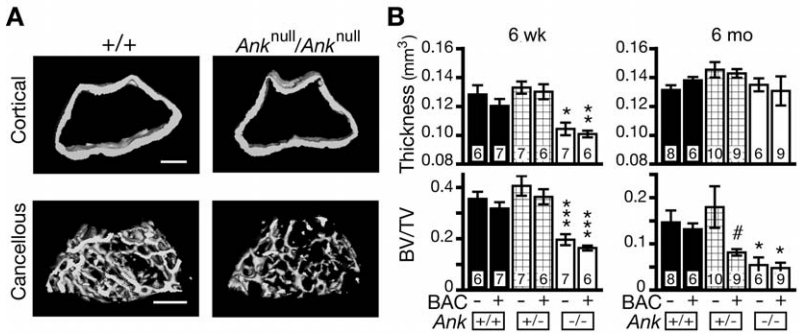

Figure 5. μCT analysis of the femur. *A,* Volumetric reconstructions of cortical and cancellous bone from the metaphysis of wild-type and mutant distal femurs. The cortex from *Ank* null mice was slightly thinner but similar in shape, whereas the cancellous bone was sparse compared with wild type. *B,* Quantified values for images in panel A for mice euthanized at age 6 wk and 6 mo. *Ank* null mice exhibited decreased metaphyseal cortical thickness at age 6 wk but not at age 6 mo. In contrast, these mice exhibited a decreased ratio of bone:tissue volume (BV:TV) relative to wild type in the metaphyseal cancellous bone at both age 6 wk and age 6 mo. Note that the presence of BAC-Ank^{G389R} had no affect on wild-type or *Ank* null mice. However, this BAC had a significant dominant negative effect on the cancellous region of $+/Ank^{null}$ mice at age 6 mo. A single asterisk (*) indicates $P < .05$; a double asterisk (**) indicates $P < .01$; a triple asterisk (***) indicates $P < .001$ versus wild-type control; a pound sign (#) indicates $P < .01$ for BAC+ versus BAC−; the number of mice analyzed is indicated at the base of each bar.

veloped for ANK-stimulated transport and for testing the activity of mutant ANK proteins.

CCAL2 Mutations

Previous studies showed that CCAL2 alleles retain at least wild-type levels of activity.[10] However, conflicting results have been described for these and other CCAL2 mutations, including reported loss of activity for both P5T and M48T.[31] Surprisingly, the same mutation (M48T) tested by two groups scored as indistinguishable from wild type in one case and as complete loss of function in the other. In both cases, assessment of ANK activity relied on measurements of bulk PPi levels surrounding and inside cells after several days of culture. Because PPi is rapidly degraded and is generated as a by-product of numerous metabolic reactions—including RNA and DNA elongation, tRNA synthesis, and fatty-acid activation—the reported changes in PPi levels after cell transfection may be the result of indirect mechanisms that are variable across different cell types and different culture conditions. We report here that both tested human CCAL2 mutations (P5T and M48T) retain substantial PPi-transport activity in radiotracer flux experiments, which take place over minutes instead of days. Both mutant proteins had an apparent affinity and a rate similar to that of the wild-type protein.

In addition, we tested the functional consequences of ANK mutations in vivo for the first time. The transgenic M48T-mutant ANK protein was able to rescue the joint-mobility defects of *Ank* null mice, confirming the functional activity of the CCAL2 alleles measured in the flux experiments. These results are consistent with previous models that CCAL2 is the result of subtle changes in ANK activity,[10,34] which may result from small changes in protein function undetected by our assay or by alterations in mRNA or protein stability or in the way ANK interacts with other proteins.

We favor the ANK gain-of-function hypothesis, in which the CCAL2 mutations lead to higher steady-state concentrations of PPi in the joint space. This is supported by both the increased levels of PPi in synovial fluid and the development of CPPD crystal deposits in patients with CCAL2. However, we have not yet been able to demonstrate activities higher than wild type, using either cell-culture or oocyte assays. In addition, the Ank^{M48T} allele restores normal joint function in *Ank* null animals but does not stimulate overall increase in mineralization, as typically seen in patients with CCAL2. Although humans and mice are very similar in most metabolic pathways, significant differences do exist.[62] To the best of our knowledge, the CPPD crystal type has never been reported in mice, and it is possible that mice do not possess the appropriate chemical environment for CPPD-crystal formation. In addition, human patients with CCAL2 are unaffected until age 30–40 years, perhaps because of wear and tear or particular types of mechanical stress. It may be impossible to mimic these conditions in the 2-year life span of a mouse. Even humans with hypophosphatasia (MIM 146300, 241510, and 241500), who experience a lifetime of systemically increased PPi levels, generally do not develop CPPD joint crystals until adulthood.[63] It is also possible that the BAC we used does not contain the *cis*-acting regulatory sequences necessary for the induction of CCAL2. However, this is unlikely, because the BAC does contain the proper sequences to drive *Ank* expression in the joints and to rescue the null phenotype[3] (and data presented here). Despite the absence of CCAL2 phenotypes in transgenic

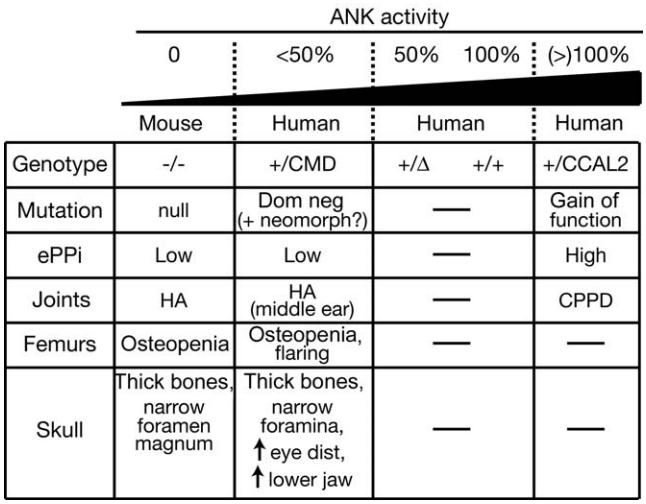

Figure 6. Range of mutations and phenotypes at the *ANKH* locus. The nature of mutations is suggested on the basis of biochemical assays and functional tests in transgenic mice. HA = hydroxyapatite crystal deposits; CPPD = CPPD crystal deposits; Dom neg = dominant negative; neomorph = neomorphic allele; eye dist = distance between the eyes.

mice, the combination of both in vitro and in vivo results clearly shows that CCAL2 alleles retain substantial activity and are not loss-of-function mutations.

CMD Mutations

It has been proposed elsewhere that CMD alleles are either "leaky" gain-of-function,[8] loss-of-function, or perhaps dominant negative mutations.[11] Our in vitro flux and in vivo transgenic rescue experiments show that, in contrast to the CCAL2 mutations, the CMD mutations (C331R and G389R) abolish or greatly reduce ANK PPi-transport activity. Co-injection experiments in frog oocytes (fig. 2*C*) and genetic tests in heterozygous *Ank* mice (fig. 5*B*) also suggest that CMD alleles have some dominant negative effects.

Previous data from heterozygous null mutations in mice and 5p deletions in human patients with cri du chat syndrome (MIM 123450) suggest that loss of one copy of the *ANKH* gene does not produce the phenotype of either CCAL2 or CMD.[25,64] ANK activity may need to be reduced to below 50% of normal to produce ectopic mineralization, which would explain the limited mutation spectrum of CMD alleles. CMD mutations are strikingly clustered within the ANK protein rather than being distributed throughout the protein, as might be expected if simple loss of ANK function were sufficient to produce CMD phenotypes.[8,11] The mechanism for the dominant negative effect of CMD alleles is currently not clear. Although the C331R mutant exhibits reduced surface expression, the wild-type, CCAL2, and CMD forms of the ANK protein all translocate to the cell surface when expressed alone (fig. 2*D*). When the C331R or G389R mutants are coexpressed in the same cell with wild-type protein, substantial levels of ANK are detected at the cell surface, whereas transport activity is markedly reduced (fig. 2*C* and 2*D*). This suggests that intracellular trapping is not the primary or only mechanism leading to reduced activity. It is possible that CMD alleles have additional effects on the specificity of ANK-transport activity, formation of ANK homomultimers, or interactions with other proteins that participate in PPi metabolism, such as ENPP1.[3,33,65,66]

If CMD is caused by the dominant negative inhibition of ANK activity, then some CMD phenotypes might be expected in animals with <50% of normal ANK activity, including Ank^{null}/Ank^{null} mice. A careful μCT examination of bone thickness and density confirmed several previously unappreciated phenotypes in *Ank* null mice that do resemble defects seen in patients with CMD, including increased thickness of a subset of skull bones, fusion of the middle-ear bones, and narrowing of the foramen magnum. Flaring of the distal femur, which is seen in humans, was not detected in mice, perhaps because of differences in the shape and mechanical loading of femurs in bipedal versus quadrapedal animals. Interestingly, we did detect a reduction in cancellous bone volume in the metaphysis of the femur of *Ank* null mice. The flared metaphysis of patients with CMD is often described as radiolucent or nonsclerotic,[49–51,67] and it has been suggested that CMD may affect the proper trabeculation of the metaphyses.[11] The loss of bone at this location in patients with CMD and *Ank* null mice is in contrast to the increased bone elsewhere in the skeleton. This may be explained by the expression of *Ank* in the growth plate and the reported role of ANK in chondrocyte hypertrophy and mineralization.[68]

The recent knockout of the *Ank* gene and the current experiments on CCAL2 and CMD alleles provide a working model for interpreting the phenotypic effects of different ANK mutations[25] (fig. 6). Animals with two copies of the *Ank* gene have normal skulls, limbs, and joints. Loss of one copy of the gene is also compatible with normal bone, presumably because either 50% or 100% of ANK activity provides sufficient PPi transport to inhibit ectopic hydroxyapatite mineral formation. The dominant negative activity of CMD alleles leads to a further reduction in ANK activity below the 50% level. At this point, some bone phenotypes begin to occur, including thickening of skull bones and narrowing of foramina. Complete loss of ANK activity triggers widespread ectopic hydroxyapatite deposition, leading to severe mineralization of joints and articular cartilage.

The dual role of PPi as both an inhibitor of hydroxyapatite formation and stimulator of calcium PPi mineral deposition leads to a different form of crystal pathology in patients with CCAL2. Unlike CMD alleles, CCAL2 alleles show significant PPi-transport activity in vitro and significant rescuing activity in transgenic mice. Slight gain-of-function mutations in ANK activity may predispose to precipitation of CPPD crystals, a phenotype seen in pa-

tients with CCAL2 by the 3rd or 4th decade of life. Synovial fluid from the knees of up to 60% of patients (average age 70 years) before arthroplasty contains CPPD and/or hydroxyapatite crystals,[69] and recent reports show elevated levels of *ANKH* expression in cartilage samples from patients with sporadic CPPD deposition.[66,70] Given the sensitivity of crystal deposition to total levels of ANK activity, modulation of this pathway may be a useful clinical target for controlling susceptibility to common mineral-deposition diseases.

Acknowledgments

We thank Roel Nusse and members of the Kingsley lab for useful discussions, Richard Aldrich for frog oocytes, and the Stanford Transgenic Core for pronuclear injections. This work was supported by a Howard Hughes Medical Institute predoctoral fellowship (to K.A.G.) and by National Institutes of Health grant AR42236 (to D.M.K.). D.M.K. is an investigator of the Howard Hughes Medical Institute.

Web Resource

The URL for data presented herein is as follows:

Online Mendelian Inheritance in Man (OMIM), http://www.ncbi.nlm.nih.gov/Omim/ (for CCAL2, CMD, hypophosphatasia, and cri du chat syndrome)

References

1. Bunger MK, Walisser JA, Sullivan R, Manley PA, Moran SM, Kalscheur VL, Colman RJ, Bradfield CA (2005) Progressive arthropathy in mice with a targeted disruption of the Mop3/Bmal-1 locus. Genesis 41:122–132
2. Heiss A, DuChesne A, Denecke B, Grotzinger J, Yamamoto K, Renne T, Jahnen-Dechent W (2003) Structural basis of calcification inhibition by α_2-HS glycoprotein/fetuin-A. Formation of colloidal calciprotein particles. J Biol Chem 278:13333–13341
3. Ho AM, Johnson MD, Kingsley DM (2000) Role of the mouse *ank* gene in control of tissue calcification and arthritis. Science 289:265–270
4. Luo G, Ducy P, McKee MD, Pinero GJ, Loyer E, Behringer RR, Karsenty G (1997) Spontaneous calcification of arteries and cartilage in mice lacking matrix GLA protein. Nature 386:78–81
5. Murshed M, Harmey D, Millan JL, McKee MD, Karsenty G (2005) Unique coexpression in osteoblasts of broadly expressed genes accounts for the spatial restriction of ECM mineralization to bone. Genes Dev 19:1093–1104
6. Murshed M, Schinke T, McKee MD, Karsenty G (2004) Extracellular matrix mineralization is regulated locally: different roles of two gla-containing proteins. J Cell Biol 165:625–630
7. Narisawa S, Frohlander N, Millan JL (1997) Inactivation of two mouse alkaline phosphatase genes and establishment of a model of infantile hypophosphatasia. Dev Dyn 208:432–446
8. Nurnberg P, Thiele H, Chandler D, Hohne W, Cunningham ML, Ritter H, Leschik G, Uhlmann K, Mischung C, Harrop K, Goldblatt J, Borochowitz ZU, Kotzot D, Westermann F, Mundlos S, Braun HS, Laing N, Tinschert S (2001) Heterozygous mutations in *ANKH,* the human ortholog of the mouse progressive ankylosis gene, result in craniometaphyseal dysplasia. Nat Genet 28:37–41
9. Okawa A, Nakamura I, Goto S, Moriya H, Nakamura Y, Ikegawa S (1998) Mutation in Npps in a mouse model of ossification of the posterior longitudinal ligament of the spine. Nat Genet 19:271–273
10. Pendleton A, Johnson MD, Hughes A, Gurley KA, Ho AM, Doherty M, Dixey J, Gillet P, Loeuille D, McGrath R, Reginato A, Shiang R, Wright G, Netter P, Williams C, Kingsley DM (2002) Mutations in *ANKH* cause chondrocalcinosis. Am J Hum Genet 71:933–940
11. Reichenberger E, Tiziani V, Watanabe S, Park L, Ueki Y, Santanna C, Baur ST, Shiang R, Grange DK, Beighton P, Gardner J, Hamersma H, Sellars S, Ramesar R, Lidral AC, Sommer A, Raposo do Amaral CM, Gorlin RJ, Mulliken JB, Olsen BR (2001) Autosomal dominant craniometaphyseal dysplasia is caused by mutations in the transmembrane protein ANK. Am J Hum Genet 68:1321–1326
12. Schafer C, Heiss A, Schwarz A, Westenfeld R, Ketteler M, Floege J, Muller-Esterl W, Schinke T, Jahnen-Dechent W (2003) The serum protein α_2-Heremans-Schmid glycoprotein/fetuin-A is a systemically acting inhibitor of ectopic calcification. J Clin Invest 112:357–366
13. Speer MY, McKee MD, Guldberg RE, Liaw L, Yang HY, Tung E, Karsenty G, Giachelli CM (2002) Inactivation of the osteopontin gene enhances vascular calcification of matrix Gla protein-deficient mice: evidence for osteopontin as an inducible inhibitor of vascular calcification in vivo. J Exp Med 196:1047–1055
14. Steitz SA, Speer MY, McKee MD, Liaw L, Almeida M, Yang H, Giachelli CM (2002) Osteopontin inhibits mineral deposition and promotes regression of ectopic calcification. Am J Pathol 161:2035–2046
15. Sweet HO, Green MC (1981) Progressive ankylosis, a new skeletal mutation in the mouse. J Hered 72:87–93
16. Waymire KG, Mahuren JD, Jaje JM, Guilarte TR, Coburn SP, MacGregor GR (1995) Mice lacking tissue non-specific alkaline phosphatase die from seizures due to defective metabolism of vitamin B-6. Nat Genet 11:45–51
17. Williams CJ, Zhang Y, Timms A, Bonavita G, Caeiro F, Broxholme J, Cuthbertson J, Jones Y, Marchegiani R, Reginato A, Russell RGG, Wordsworth BP, Carr AJ, Brown MA (2002) Autosomal dominant familial calcium pyrophosphate dihydrate deposition disease is caused by mutation in the transmembrane protein ANKH. Am J Hum Genet 71:985–991
18. Fleisch H, Bisaz S (1962) Isolation from urine of pyrophosphate, a calcification inhibitor. Am J Physiol 203:671–675
19. Fleisch H, Bisaz S (1962) Mechanism of calcification: inhibitory role of pyrophosphate. Nature 195:911
20. Derfus BA, Rachow JW, Mandel NS, Boskey AL, Buday M, Kushnaryov VM, Ryan LM (1992) Articular cartilage vesicles generate calcium pyrophosphate dihydrate-like crystals in vitro. Arthritis Rheum 35:231–240
21. Mandel GS, Halverson PB, Rathburn M, Mandel NS (1990) Calcium pyrophosphate crystal deposition: a kinetic study using a type I collagen gel model. Scanning Microsc 4:175–180
22. Mandel NS, Mandel GS, Carroll DJ, Halverson PB (1984) Calcium pyrophosphate crystal deposition: an in vitro study using a gelatin matrix model. Arthritis Rheum 27:789–796
23. Hakim FT, Cranley R, Brown KS, Eanes ED, Harne L, Oppenheim JJ (1984) Hereditary joint disorder in progressive an-

kylosis (ank/ank) mice. I. Association of calcium hydroxyapatite deposition with inflammatory arthropathy. Arthritis Rheum 27:1411–1420
24. Sampson HW (1988) Ultrastructure of the mineralizing metacarpophalangeal joint of progressive ankylosis (ank/ank) mice. Am J Anat 182:257–269
25. Gurley KA, Chen H, Guenther C, Nguyen ET, Rountree RB, Schoor M, Kingsley DM (2006) Mineral formation in joints caused by complete or joint-specific loss of ANK function. J Bone Miner Res 21:1238–1247
26. Malkin I, Dahm S, Suk A, Kobyliansky E, Toliat M, Ruf N, Livshits G, Nurnberg P (2005) Association of ANKH gene polymorphisms with radiographic hand bone size and geometry in a Chuvasha population. Bone 36:365–373
27. Timms AE, Zhang Y, Bradbury L, Wordsworth BP, Brown MA (2003) Investigation of the role of *ANKH* in ankylosing spondylitis. Arthritis Rheum 48:2898–2902
28. Tsui FW, Tsui HW, Cheng EY, Stone M, Payne U, Reveille JD, Shulman MJ, Paterson AD, Inman RD (2003) Novel genetic markers in the 5′-flanking region of *ANKH* are associated with ankylosing spondylitis. Arthritis Rheum 48:791–797
29. Tsui HW, Inman RD, Paterson AD, Reveille JD, Tsui FW (2005) *ANKH* variants associated with ankylosing spondylitis: gender differences. Arthritis Res Ther 7:R513–R525
30. Williams CJ, Pendleton A, Bonavita G, Reginato AJ, Hughes AE, Peariso S, Doherty M, McCarty DJ, Ryan LM (2003) Mutations in the amino terminus of ANKH in two US families with calcium pyrophosphate dihydrate crystal deposition disease. Arthritis Rheum 48:2627–2631
31. Zhang Y, Johnson K, Russell RG, Wordsworth BP, Carr AJ, Terkeltaub RA, Brown MA (2005) Association of sporadic chondrocalcinosis with a -4-basepair G-to-A transition in the 5′-untranslated region of *ANKH* that promotes enhanced expression of ANKH protein and excess generation of extracellular inorganic pyrophosphate. Arthritis Rheum 52:1110–1117
32. Harmey D, Hessle L, Narisawa S, Johnson KA, Terkeltaub R, Millan JL (2004) Concerted regulation of inorganic pyrophosphate and osteopontin by akp2, enpp1, and ank: an integrated model of the pathogenesis of mineralization disorders. Am J Pathol 164:1199–1209
33. Johnson K, Goding J, Van Etten D, Sali A, Hu SI, Farley D, Krug H, Hessle L, Millan JL, Terkeltaub R (2003) Linked deficiencies in extracellular PP(i) and osteopontin mediate pathologic calcification associated with defective PC-1 and ANK expression. J Bone Miner Res 18:994–1004
34. Costello JC, Ryan LM (2004) Modulation of chondrocyte production of extracellular inorganic pyrophosphate. Curr Opin Rheumatol 16:268–272
35. Williams CJ (2003) Familial calcium pyrophosphate dihydrate deposition disease and the ANKH gene. Curr Opin Rheumatol 15:326–331
36. Doherty M, Hamilton E, Henderson J, Misra H, Dixey J (1991) Familial chondrocalcinosis due to calcium pyrophosphate dihydrate crystal deposition in English families. Br J Rheumatol 30:10–15
37. Lee EC, Yu D, Martinez de Velasco J, Tessarollo L, Swing DA, Court DL, Jenkins NA, Copeland NG (2001) A highly efficient *Escherichia coli*-based chromosome engineering system adapted for recombinogenic targeting and subcloning of BAC DNA. Genomics 73:56–65
38. Hildebrand T, Laib A, Muller R, Dequeker J, Ruegsegger P (1999) Direct three-dimensional morphometric analysis of human cancellous bone: microstructural data from spine, femur, iliac crest, and calcaneus. J Bone Miner Res 14:1167–1174
39. Hildebrand T, Rüegsegger P (1997) A new method for the model-independent assessment of thickness in three-dimensional images. J Microsc 185:67–75
40. Laib A, Barou O, Vico L, Lafage-Proust MH, Alexandre C, Rugsegger P (2000) 3D micro-computed tomography of trabecular and cortical bone architecture with application to a rat model of immobilisation osteoporosis. Med Biol Eng Comput 38:326–332
41. Cass CE, Young JD, Baldwin SA (1998) Recent advances in the molecular biology of nucleoside transporters of mammalian cells. Biochem Cell Biol 76:761–770
42. Chaudhry FA, Reimer RJ, Krizaj D, Barber D, Storm-Mathisen J, Copenhagen DR, Edwards RH (1999) Molecular analysis of system N suggests novel physiological roles in nitrogen metabolism and synaptic transmission. Cell 99:769–780
43. Corbel S, Dy M (1996) Evidence for bidirectional histamine transport by murine hematopoietic progenitor cells. FEBS Lett 391:279–281
44. Jonker JW, Schinkel AH (2004) Pharmacological and physiological functions of the polyspecific organic cation transporters: OCT1, 2, and 3 (SLC22A1-3). J Pharmacol Exp Ther 308:2–9
45. Mancini GM, de Jonge HR, Galjaard H, Verheijen FW (1989) Characterization of a proton-driven carrier for sialic acid in the lysosomal membrane: evidence for a group-specific transport system for acidic monosaccharides. J Biol Chem 264: 15247–15254
46. Neuhoff S, Ungell AL, Zamora I, Artursson P (2005) pH-Dependent passive and active transport of acidic drugs across Caco-2 cell monolayers. Eur J Pharm Sci 25:211–220
47. Pisoni RL, Flickinger KS, Thoene JG, Christensen HN (1987) Characterization of carrier-mediated transport systems for small neutral amino acids in human fibroblast lysosomes. J Biol Chem 262:6010–6017
48. Pisoni RL, Thoene JG, Lemons RM, Christensen HN (1987) Important differences in cationic amino acid transport by lysosomal system c and system y+ of the human fibroblast. J Biol Chem 262:15011–15018
49. Rimoin DL, Woodruff SL, Holman BL (1969) Craniometaphyseal dysplasia (Pyle's disease): autosomal dominant inheritance in a large kindred. Birth Defects 4:96–104
50. Taylor DB, Sprague P (1989) Dominant craniometaphyseal dysplasia—a family study over five generations. Australas Radiol 33:84–89
51. Beighton P (1995) Craniometaphyseal dysplasia (CMD), autosomal dominant form. J Med Genet 32:370–374
52. Gorlin RJ, Spranger J, Koszalka MF (1969) Genetic craniotubular bone dysplasias and hyperostoses: a critical analysis. Birth Defects 4:79–95
53. Stool SE, Caruso VG (1973) Cranial metaphyseal dysplasia: otolaryngologic aspects. Arch Otolaryngol 97:410–412
54. Doherty M, Belcher C, Regan M, Jones A, Ledingham J (1996) Association between synovial fluid levels of inorganic pyrophosphate and short term radiographic outcome of knee osteoarthritis. Ann Rheum Dis 55:432–436
55. Hamilton E, Pattrick M, Doherty M (1991) Inorganic pyrophosphate, nucleoside triphosphate pyrophosphatase, and car-

tilage fragments in normal human synovial fluid. Br J Rheumatol 30:260–264
56. Pattrick M, Hamilton E, Hornby J, Doherty M (1991) Synovial fluid pyrophosphate and nucleoside triphosphate pyrophosphatase: comparison between normal and diseased and between inflamed and non-inflamed joints. Ann Rheum Dis 50: 214–218
57. Ryan LM, Kozin F, McCarty DJ (1979) Quantification of human plasma inorganic pyrophosphate. I. Normal values in osteoarthritis and calcium pyrophosphate dihydrate crystal deposition disease. Arthritis Rheum 22:886–891
58. Fleisch H, Neuman W (1961) Mechanisms of calcification: role of collagen, polyphosphates, and phosphatase. Am J Physiol 200:1296
59. Johnson K, Terkeltaub R (2005) Inorganic pyrophosphate (PPI) in pathologic calcification of articular cartilage. Front Biosci 10:988–997
60. Mandel NS, Mandel GS (1984) A model for human calcium pyrophosphate crystal deposition disease: crystallization kinetics in a gelatin matrix. Scan Electron Microsc (Pt 4):1779–1792
61. Ryan LM, Kurup IV, Derfus BA, Kushnaryov VM (1992) ATP-induced chondrocalcinosis. Arthritis Rheum 35:1520–1525
62. Bedell MA, Largaespada DA, Jenkins NA, Copeland NG (1997) Mouse models of human disease. Part II: Recent progress and future directions. Genes Dev 11:11–43
63. Caswell AM, Whyte MP, Russell RG (1991) Hypophosphatasia and the extracellular metabolism of inorganic pyrophosphate: clinical and laboratory aspects. Crit Rev Clin Lab Sci 28:175–232
64. Zhang X, Snijders A, Segraves R, Zhang X, Niebuhr A, Albertson D, Yang H, Gray J, Niebuhr E, Bolund L, Pinkel D (2005) High-resolution mapping of genotype-phenotype relationships in cri du chat syndrome using array comparative genomic hybridization. Am J Hum Genet 76:312–326
65. Hosoda Y, Yoshimura Y, Higaki S (1981) A new breed of mouse showing multiple osteochondral lesions—twy mouse. Ryumachi Suppl 21:157–164
66. Johnson K, Terkeltaub R (2004) Upregulated ank expression in osteoarthritis can promote both chondrocyte MMP-13 expression and calcification via chondrocyte extracellular PPi excess. Osteoarthritis Cartilage 12:321–335
67. Lejeune E, Anjou A, Bouvier M, Robert J, Vauzelle JL, Jeanneret J (1966) [Familial cranio-metaphyseal dysplasia]. Rev Rhum Mal Osteoartic 33:714–726
68. Wang W, Xu J, Du B, Kirsch T (2005) Role of the progressive ankylosis gene (ank) in cartilage mineralization. Mol Cell Biol 25:312–323
69. Derfus BA, Kurian JB, Butler JJ, Daft LJ, Carrera GF, Ryan LM, Rosenthal AK (2002) The high prevalence of pathologic calcium crystals in pre-operative knees. J Rheumatol 29:570–574
70. Hirose J, Ryan LM, Masuda I (2002) Up-regulated expression of cartilage intermediate-layer protein and ANK in articular hyaline cartilage from patients with calcium pyrophosphate dihydrate crystal deposition disease. Arthritis Rheum 46:3218–3229